Winter Precipitations of Northern Part of Farming-pastoral Zone and Hulunbuir Grassland

You Xia (sunlight805@outlook.com)
Sun Yat-Sen University

Article

Keywords: high precipitations, atmospheric circulation, northern China

Posted Date: August 24th, 2021

DOI: https://doi.org/10.21203/rs.3.rs-828686/v1

Abstract

In January 2018 a high record of monthly total precipitation in northern China drew our attention. This number is 4 times more than that in normal winters over the past 30 years, and its location is in northern China. Thus our research region is composed by the northern part of the farming-pastoral zone and the Hulunbuir Grassland. We target our research at understanding the phenomena and causes of such high precipitations. We explore the heavy precipitation locations, and use dynamical analyses on different pressure levels to find out the cause of the high score. We analyze wind fields, geopotential heights and relative humidity for the pressure levels of 200 hPa, 500 hPa, 700 hPa and 850 hPa. We find that the location of the highest monthly total precipitation in January 2018 is on the mountain, whereas the spots of heavy precipitations during one event are not located on the mountain. Zooming in January 2018, it is the precipitation frequency that drastically increased, not the number of heavy precipitation events. The dynamical analyses show that the heavy precipitation events in January 2018 are mainly caused by appearance of cyclones either in or near the research region at high geopotential heights.

1. Introduction

Northern China is always considered as a dry region comparing to the southern China. Especially in winter, a dry lasting cold weather dominates in the north. However, January 2018 is ripe for precipitations. Our research region, called Region hereafter, is defined by the rectangle limitation comprising northern part of the farming-pastoral ecotone and Hulunbuir Grassland, because both of the mentioned areas are economically relied on winter precipitations for crops growth, pasturage and tourism business. Over the past 30 years from 1988 to 2018, the maximum winter precipitation amount of the Region is no more than 100 mm, meanwhile in January 2018 that exceeds 400 mm. This abnormal phenomenon attracts our attention. For winter heavy precipitations, several studies are investigated worldwide. Single winter heavy precipitation occurred in central Japan in January 2016. It is found that the occluding cyclones are the main cause of the heavy precipitations (Sawada et al. 2019). Cold air out breaks, passing by of extratropical cyclones are also causes of winter heavy precipitations in Japan (Kawase et al. 2018). In addition, typical winter monsoon pressure patterns also contribute to the inland heavy precipitations in Japan (Ueno and Ando 2015). Along the coast of the Sea of Japan, local-scale depressions and local convergences caused by land breezes are factors for heavy winter precipitations (Eito et al. 2005). Studies on heavy winter precipitations in Japan caused by extratropical cyclones further provide information on root causes. The result is that the combination of the warm conveyor belt, the cold conveyor belt and the dry air intrusion is vital in the contribution of the heavy precipitations (Sawada and Ueno 2021). Moving to areas above the southeast Canada and the northeast United States, North Atlantic Oscillation is the major cause of the heavy winter precipitation. The positive North Atlantic Oscillation induces less precipitations, while the negative North Atlantic Oscillation causes twice as many heavy precipitation events as the former (Chartrand and Pausata 2020). In eastern Canada, studies show that the winter precipitations are poorly correlated with the North Atlantic Oscillation (Stone et al. 2000; Bonsal and Shabbar 2008; Whan and Zwiers 2017). In aspect of sea surface temperature influences, existing

studies show that the mesoscale of that can give a remote influence on atmospheric river landfalling, leading to heavy precipitations along the west coast of North America (Liu et al. 2021). In addition, heavy winter precipitations in the west mountainous topography of America is also caused by the moisture originating from the Pacific, and transporting upwards through the mountains (Alexander et al. 2015) (Akbari Azirani et al. 2016). For a heavy precipitation event in January 2008 in Iran, a deep low trough above the north of the Caspian Sea caused by a blocking system drives the thermal and moisture gradients (Akbari Azirani et al. 2016). For summer heavy precipitations in Utah, both direct and indirect synoptic factors are important. Moreover, the humidity shift above the Atlantic Ocean plays a crucial role (Harnack et al. 1998). In Romania, positive North Atlantic Oscillation and blocking phenomenon over the Atlantic-European sector can cause winter precipitations to decrease (Tomozeiu et al. 2005). Global warming is another key contributor to extratropical cyclones, leading to the increase of the precipitation intensity (Kodama et al. 2019). Despite studies on heavy winter precipitations are done at a global scale, no studies have focused on inland winter precipitations in the areas in northern China. Moreover, the cold days can even expand up to half of a year, and the precipitation amount is much small comparing to rich moisture areas such as southern China. Hence, rare effort is investigated in the winter precipitations in the Region which locates in the north part of China. We target our research at exploring precipitation phenomena in January 2018 in the Region, and using dynamical analyses to find out the causes of such precipitations. First, we explore the trend of the Region-averaged monthly total precipitations over the recent 30 years without that of January 2018. Second, we study the location of the monthly total precipitations of Januaries in the recent 7 winters. Third, the hourly precipitations within the month are explored. The precipitation rate that exceeds 2 mm/h is defined as “heavy precipitation events” for the Region. Lastly, we focus on typical individual heavy precipitation event in January 2018, and use dynamical analyses to investigate in the atmospheric circulations during those precipitations.

2. Data And Methodology

a. Definition of the research Region

The Region comprises the north part of the farming-pastoral ecotone of China and Hulunbuir Grassland. It is a rectangle area limited by the union of the longitudes and latitudes of the ecotone and the grassland. This rectangle area helps us to understand better conditions of the precipitations and atmospheric circulations, than limiting our sights only on the banding field of ecotone and the square of grassland. The Northern part of Chinese farming-pastoral zone covers 36°30’N - 46°42’ N and 106°16’E - 124°51’E (Guo et al. 2013). The boundary of the Hulunbuir Grassland is limited by towns of Xinbaerhuyouqi, Xinbaerhuzuoqi, Chenbaerhuqi, Ewenkeqi, Hailarqu, Manzhouli, Yakeshishi, Eergunashi. Those towns encircle an area with latitude 48°N - 51°N and longitude 116.5°E - 121°E. Hence, the Region is defined by 36°N – 51°N and 106°E – 125°E.

b. Data source

All data used in this research are publicly available. The data of Monthly Total precipitations (SURF_CLI_CHN_PRE_MON_GRID_0.5) have 0.5° * 0.5° horizontal resolution, and they are taken from National Atmospheric Science Data Center of China (http://data.cma.cn/data/cdcdetail/dataCode/SURF_CLI_CHN_PRE_MON_GRID_0.5.html).

From European Centre for Medium Range Weather forecasts (ECMWF), ERA5 data is used with temporal resolution of 6 hours, and the horizontal resolution is 1*1 for hourly precipitation, 0.1*0.1 for geopotential, U and V components of wind and specific humidity at 200hPa, 500hPa 700hPa and 850hPa.

c. Methods

The hourly precipitation rate is taken as the maximum precipitation amount gleaned in the Region from January 1st 0:00 to 31th 18:00 with time resolution of 6 hours. Then “heavy” precipitation hourly rate is defined by 2 mm/h because this value can separate clearly continuous precipitation fold line into individual precipitation events, to give more convenience to our analyses. The dynamical analyses include relative humidity, wind field, geopotential height to explore atmospheric circulation above the Region during each heavy precipitation event.

3. Precipitation Phenomena

3.1 Precipitation trends

The Region locates in the north part of China, and it is renowned for cold lasting winter days and small amount of precipitations. In our research we only consider the months with the lowest temperature of a year, that is we take December, January and February as winter months. For the recent 30 winters from December 1988 to February 2018, the Regional maximum monthly total precipitations is drawn on Figure 1. The maximum precipitation values oscillate between 0 mm and 100 mm with a stable behavior, except the instance of January 2018 which exceeds 400 mm. For the Region-average precipitation, the value of January 2018 is about three times higher than that of normal months.

To see where the value of the maximum precipitation in January 2018 situates through the 30 winters, we draw on Figure 2 Region-averaged and maximum monthly total precipitation using GEV distribution. The Region-averaged monthly total precipitation in dark blue line is centered at 4 mm, and the probability falls to 0 at 15 mm. For the maximum monthly total precipitation in cyan color, the maximum probability locates at 25 mm, and it equals to 0 for precipitation value larger than 150 mm. This means the precipitation value of January 2018 is unprecedented in history.

To understand precipitation trend of the Region, the Region-averaged monthly total precipitation for the 30 winters is drawn on Figure 3. Only in December 1990 the Region-averaged precipitation value is more than 10 mm, while for other months, this value never exceeds 8 mm. The slope of the trend line is positive, which means the precipitation amount is increasing in the Region. The small value of the slope expresses the tiny amount of growth. We can think of the precipitations of the Region as in a stable state.

3.2 Precipitation locations

For the recent 30 years, the locations of the maximum monthly total precipitation of the Region are mainly separated to five sites. These precipitations are named after those sites: East border precipitation, Northeast precipitation, Southwest precipitation, Coastal precipitation and Inland precipitation.

The precipitations of January 1997 shown on Figure 4 is a typical case for East border precipitation because its maximum monthly total precipitation locates at the east border of the Region. More precisely the precipitation is in Liaoning province, the south part of Changbai Mountain. The maximum precipitation value is around 20 mm.

On Figure 5, the precipitations of January 2002 stands for Northeast precipitation since its highest monthly total precipitation is in the northeast corner of the Region. It locates within 47 °N – 51 °N, 116 °E – 125 °E. This area is within Inner Mongolia, in the north part of Daxinganling Mountain. The precipitation amount ranges from 20 mm to 40 mm.

Figure 6 shows the precipitations of January 2008 which illustrates Southwest precipitation. The precipitation covers the area of 36 °N – 40 °N, 106 °E – 112 °E, which is mainly in the north part of the farming-pastoral ecotone without reaching up to Hebei, Beijing or Tianjin. This is in the Liupanshan Mountain.

The precipitations in January 2017 on Figure 7 illustrate Coastal precipitation because the maximum precipitation location is within the east part of Shandong province with 36 °N – 38 °N, 118 °E – 123 °E. This is the only part that thrusts into the ocean, with a topography of plain.

The precipitations on Figure 8 stands for Inland precipitations, and they occurred in January 2018. Those precipitations are typical because they cover a band area from 112 °E 36 °N to 122 °E 51 °N with a linear line shape. The dark green color on the figure shows that the precipitation amount is largely saturated by the limit of 100 mm as shown on the color bar to the right of the figure. The use of this limit aims at firstly highlight the significance of the precipitation amount in January 2018, secondly be consistent with the scale of other figures. Those precipitations mainly locate in Shanxi, Northwest of Hebei and Northeast of Inner Mongolia provinces. The topography there are mountainous, including from south to north Taihangshan Mountain, west part of Yinshan Mountain and the whole length of Daxinganling Mountain.

3.3 Precipitation rate

Since we find that from 1988 to 2018 the winter precipitations are stable, we focus only on precipitations in Januaries from 2012 to 2018. We need to know individual heavy precipitation event in the month to get more details about the phenomena, thus precipitation per hour is drawn for Januaries from 2012 to 2018 on Figure 9 as (a) to (g). The precipitations which have rates exceeding 2 mm/h are chosen as “heavy” precipitations of the Region, because this rate value can clearly separate individual precipitation event within one month, in order to extract relative heavy precipitations. It should be noted that for one precipitation event, the time interval of non-precipitating should be less than 24 hours. There are 5 heavy

precipitation events for 2012; 3 events for 2013; 7 events for 2014; 6 events for 2015; 8 events for 2016; 5 events for 2017 and 7 events for 2018. Among those precipitations, in January 2013 and 2017 precipitations have extreme values.

Figure 10 illustrates the sum of the heavy precipitation duration for each January from 2012 to 2018. The January 2018 has the longest duration, which corresponds to 260 hours. The January 2013 has the minimum duration, that is 90 hours. The growth of the heavy precipitation hours is obvious from 2013 to 2018. However, the months with the peak precipitations such as January 2013 and January 2017 do not have the largest precipitation duration hours. Thus, for January 2018 it is the precipitation frequency which drastically increased comparing to other months, which makes it the longest precipitation month.

4. Precipitation Analyses Of The Region

The heavy precipitation events in January 2018 of the Region are analyzed in details, concluding the precipitation locations and the atmospheric circulations.

4.1 Precipitation locations

According to the locations of the precipitations, there are five types of events: Northeast precipitation, Southwest precipitation, West to east precipitation, East border precipitation and Inland precipitation. For the precipitations with the same names as previously illustrated examples, the precipitation locations within the Region are the same. The five types of precipitations are shown on Figure 11. For the Northeast precipitation, the highest precipitation is in the northeast corner of the Region. The wind steps down from the north, and a trough is to the southeast of Japan, on the Pacific. The Southwest precipitation has relative high geopotential height comparing to the northeast corner in the Region. The West to east precipitation has many precipitation spots dispersing over the whole Region. The geopotential height is also higher in the southwest corner and lower in the northeast corner of the Region. For the East border precipitation, the precipitations in the Region is centralized at the east border to the Region. An low pressure trough is above the Sea of Japan. Finally, the Inland precipitation has a trough with its center at 118 °E 46 °N. The geopotential height is high to the south and low to the north.

4.2 Atmospheric circulation patterns

The atmospheric circulation for the Northeast precipitation is shown on Figure 12. At 200 hPa the Region is dominated by west wind. At 500 hPa two cyclones are created, the first one is at 88 °E 48 °N, and the second is at 131 °E 45 °N. The northeast corner of the Region is mainly dominated by north wind induced by the second cyclone. Despite at 700 hPa the two cyclones are subdued, the northeast corner of the Region is still influenced by the north wind. At 850 hPa the first cyclone looses its pattern, while the second cyclone persists. Through the whole precipitation event, at 500 and 700 hPa a cyclone centered at 122 °E 48 °N is moving towards the second cyclone, and merges with it. At 850 hPa this moving cyclone does not appear. The second cyclone occludes throughout the precipitation event above the Sea of

Japan. The Northeast precipitation of the Region is caused by the occluding cyclone above the Sea of Japan.

The Southwest precipitation is shown on Figure 13. At 200 hPa the west wind dominates in the Region. At 500 hPa a cyclone at 85 °E 46 °N appears, and its flow pattern influences the wind field in the Region. At 20 °N, 90 °E – 110 °E strong southwest wind with moisture intrudes into the Region. Combining the influence induced by the cyclone, the southwest and the northwest wind interact inside the Region. At 700 hPa, the cyclone is subdued and the influence inside the Region disappears. A strong south wind with relative high moisture blows into the southwest corner of the Region, confronting the north dry wind. At 850 hPa, the south wind is pushed southward by the north dry wind, only remaining in the southwest corner of the Region. Throughout the precipitation event, no significant persisting cyclones are present. Instead, the remarkable invasion of the south wind with high moisture into the southwest corner of the Region which dominated by north dry wind, causes the Southwest precipitation.

Figure 14 illustrate the West to east precipitation. At 200 hPa, the Region is dominated by west wind. At 500 hPa a convergence appears at 110 °E 44 °N in the central part of the Region. Stepping downward to 700 and 850 hPa, the convergence is gradually weakening until loosing its patterns. This convergence is in forms of a cyclone at 500 and 700 hPa at the beginning hours of the precipitation. As it moves eastward, it looses its cyclone patterns progressively. At 850 hPa, no significant cyclone features are observed. This West to east precipitation is due to convergence caused by pressure pattern in the atmosphere.

The East border precipitations is represented on Figure 15. At 200 hPa, northwest wind is prominent in the Region. At 500 and 700 hPa, north wind dominates, and a cyclone without clear patterns is formed at 133 °E 45 °N, near the Sea of Japan. At 850 hPa, that cyclone enforced its patterns, and it locates just above the Sea of Japan. During the precipitations, the cyclone above the Sea of Japan only appears at ground level. Consequently, the East border precipitation is caused by the cyclone above the Sea of Japan.

The Inland precipitation is shown on Figure 16. From 200 to 700 hPa the west wind dominates in the Region. A slight curvature of the geopotential line appears at 500 hPa at 115 °E 46 °N and enhances downward until 850 hPa to form a small cyclone. During the precipitation, at 200 and 500 hPa the Region is dominated by west wind. At 700 hPa, strong southwest wind invades the Region, interacting with west wind. This interaction leads to a small convergence in the wind field. At 850 hPa, a small inland cyclone is formed due to the active interactions of the two winds. That is, the Inland precipitation is caused by a ground breeze induced small cyclone.

5. Discussion

The five precipitation types in January 2018 are Northeast precipitation, Southwest precipitation, West to east precipitation, East border precipitation and Inland precipitation. Among the precipitations, the Northeast precipitation is caused by occluding cyclone above the Sea of Japan, while the East border

precipitation is induced by the same cyclone but formed at sea level. The Southwest precipitation is wrought by the frontal effects between southwest moist wind and the northwest dry wind. The West to east precipitation is due to the change of pressure pattern inside the Region, and the Inland precipitation is induced by ground breezes.

Comparing to other typical precipitations through the 30 winters, the Coastal precipitation in January 2017 is not seen, while the West to east precipitation and Inland precipitation are additional types in January 2018. The former can also be contributed to existence of cyclones above the ocean surface because of its location, and the latter is mainly due to the pressure change and local breezes of the Region. We recall that in January 2018, it is the heavy precipitation frequency that increases, rather than the number of extreme precipitation events. Thus, the high precipitation amount in January 2018 is caused by active atmospheric circulation above the Region.

6. Conclusion

For the Region in January 2018, the maximum of the monthly total precipitation is 4 times more than that in other winter months for the recent 30 years. The precipitations in January 2018 is mainly concentrated along the mountainous land. To see more in details, it is the heavy precipitation frequency rather than the number of extreme precipitation events that increases drastically. For these precipitations, there are five major types named after their locations: Northeast precipitation, Southwest precipitation, West to east precipitation, East border precipitation and Inland precipitation. The Northeast precipitation and the East border precipitation are both induced by cyclones above the Sea of Japan, but the former is caused by an occluding cyclone while the latter by a small cyclone formed at sea level. The Southwest precipitation is frontal precipitation between southwest moist wind and northwest dry wind. The West to east precipitation is generated by the change of atmospheric pressure above the Region, and the Inland precipitation is risen by ground breezes. The high precipitation amount in January 2018 is resulted from active atmospheric circulation.

Declarations

Acknoledgement

All data used are publicly available, and no funding is received for this research.

Declarations

No funding is received for this research. There is no conflict of interest. All data are publicly available. Python is used for coding.

References

Akbari Azirani, T., G. Azizi, A. Asadi, and M. Davoudi, 2016: The role of blocking system in heavy precipitation of Iran (a case study: southeast of Iran January 2008). *Arab. J. Geosci.*, **9**, 1–15, https://doi.org/10.1007/s12517-016-2588-2.

Alexander, M. A., J. D. Scott, D. Swales, M. Hughes, K. Mahoney, and C. A. Smith, 2015: Moisture Pathways into the U.S. Intermountain West Associated with Heavy Winter Precipitation Events. *J. Hydrometeorol.*, **16**, 1184–1206, https://doi.org/10.1175/JHM-D-14-0139.1.

Bonsal, B., and A. Shabbar, 2008: Impacts of Large-Scale Circulation Variability on Low Streamflows over Canada: A Review. *Can. Water Resour. J. Rev. Can. Ressour. Hydr.*, **33**, 137–154, https://doi.org/10.4296/cwrj3302137.

Chartrand, J., and F. S. R. Pausata, 2020: Impacts of the North Atlantic Oscillation on winter precipitations and storm track variability in southeast Canada and the northeast United States. *Weather Clim. Dyn.*, **1**, 731–744, https://doi.org/10.5194/wcd-1-731-2020.

Eito, H., T. Kato, M. Yoshizaki, and A. Adachi, 2005: Numerical Simulation of the Quasi-Stationary Snowband Observed over the Southern Coastal Area of the Sea of Japan on 16 January 2001. *J. Meteorol. Soc. Jpn. Ser II*, **83**, 551–576, https://doi.org/10.2151/jmsj.83.551.

Harnack, R. P., D. T. Jensen, and J. R. Cermak III, 1998: Investigation of upper-air conditions occurring with heavy summer rain in Utah. *Int. J. Climatol.*, **18**, 701–723, https://doi.org/10.1002/(SICI)1097-0088(19980615)18:7<701::AID-JOC265>3.0.CO;2-S.

Kawase, H., and Coauthors, 2018: Characteristics of Synoptic Conditions for Heavy Snowfall in Western to Northeastern Japan Analyzed by the 5-km Regional Climate Ensemble Experiments. *J. Meteorol. Soc. Jpn. Ser II*, **96**, 161–178, https://doi.org/10.2151/jmsj.2018-022.

Kodama, C., B. Stevens, T. Mauritsen, T. Seiki, and M. Satoh, 2019: A New Perspective for Future Precipitation Change from Intense Extratropical Cyclones. *Geophys. Res. Lett.*, **46**, 12435–12444, https://doi.org/10.1029/2019GL084001.

Liu, X., and Coauthors, 2021: Ocean fronts and eddies force atmospheric rivers and heavy precipitation in western North America. *Nat. Commun.*, **12**, 1–10, https://doi.org/10.1038/s41467-021-21504-w.

Sawada, M., and K. Ueno, 2021: Heavy Winter Precipitation Events with Extratropical Cyclone Diagnosed by GPM Products and Trajectory Analysis. *J. Meteorol. Soc. Jpn. Ser II*, 2021–2024, https://doi.org/10.2151/jmsj.2021-024.

——, R. Anzai, and K. Ueno, 2019: Continuous heavy precipitation with a winter occluding cyclone captured by GPM satellite in central Japan.

Stone, D. A., A. J. Weaver, and F. W. Zwiers, 2000: Trends in Canadian precipitation intensity. *Atmosphere-Ocean*, **38**, 321–347, https://doi.org/10.1080/07055900.2000.9649651.

Tomozeiu, R., S. Stefan, and A. Busuioc, 2005: Winter precipitation variability and large-scale circulation patterns in Romania. *Theor. Appl. Climatol.*, **81**, 193–201, https://doi.org/10.1007/s00704-004-0082-3.

Ueno, K., and N. Ando, 2015: Occurence Tendency of Heavy Rainfall or Snowfall in the Inland District of Japan in Winter. *Seppyo*, **77**, 397–410.

Whan, K., and F. Zwiers, 2017: The impact of ENSO and the NAO on extreme winter precipitation in North America in observations and regional climate models. *Clim. Dyn.*, **48**, 1401–1411, https://doi.org/10.1007/s00382-016-3148-x.

Figures

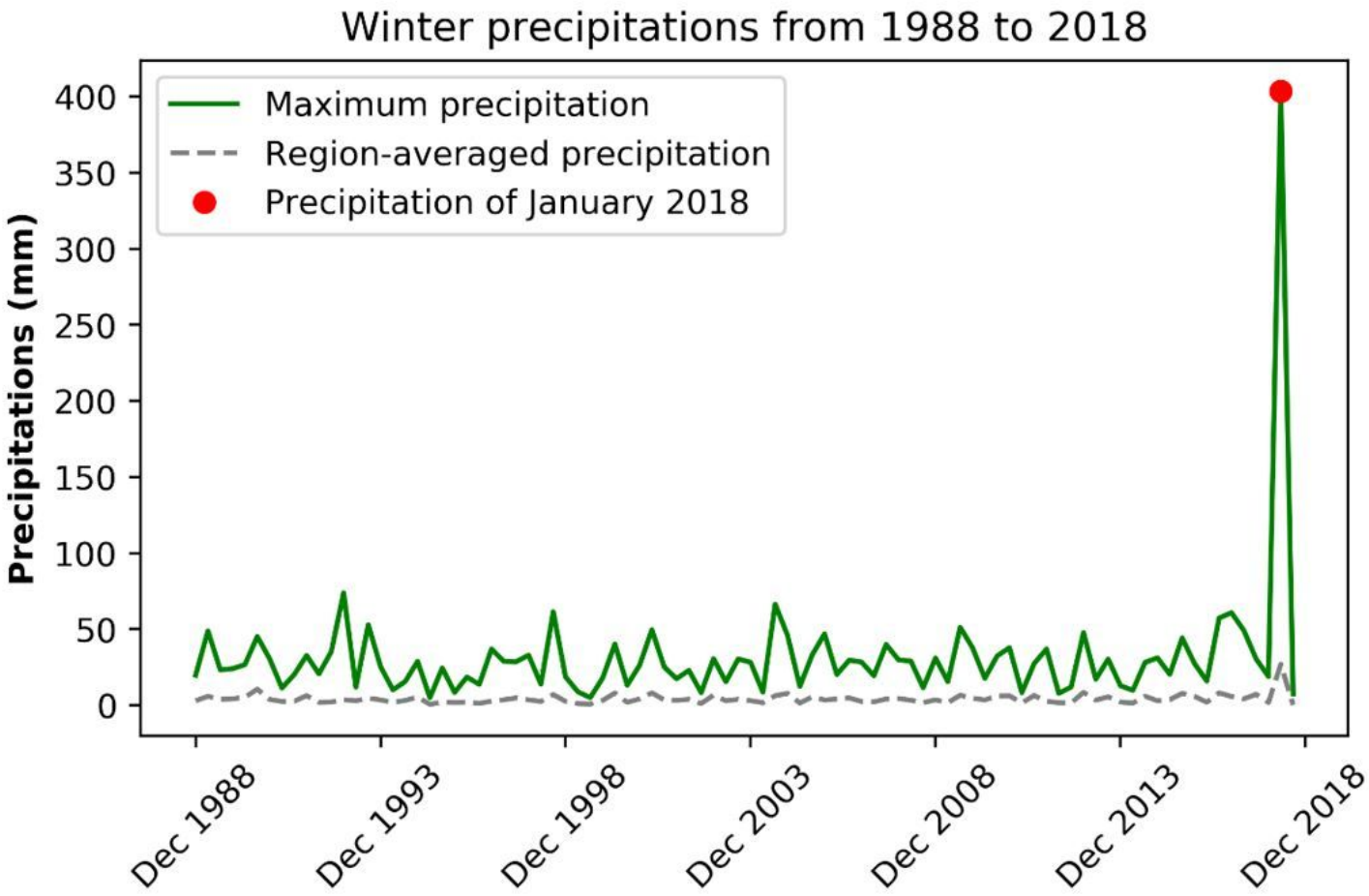

Figure 1

Regional maximum values of monthly total precipitations for recent 30 winters from December 1988 to February 2018 for the months December, January and February. The horizontal axis is time line and the vertical axis is precipitation amount with units of mm. The green solid line is Regional maximum monthly total precipitation value, and the gray dashed line is the Region-averaged monthly total precipitation. The red spot is the Regional maximum monthly total precipitation value of January 2018.

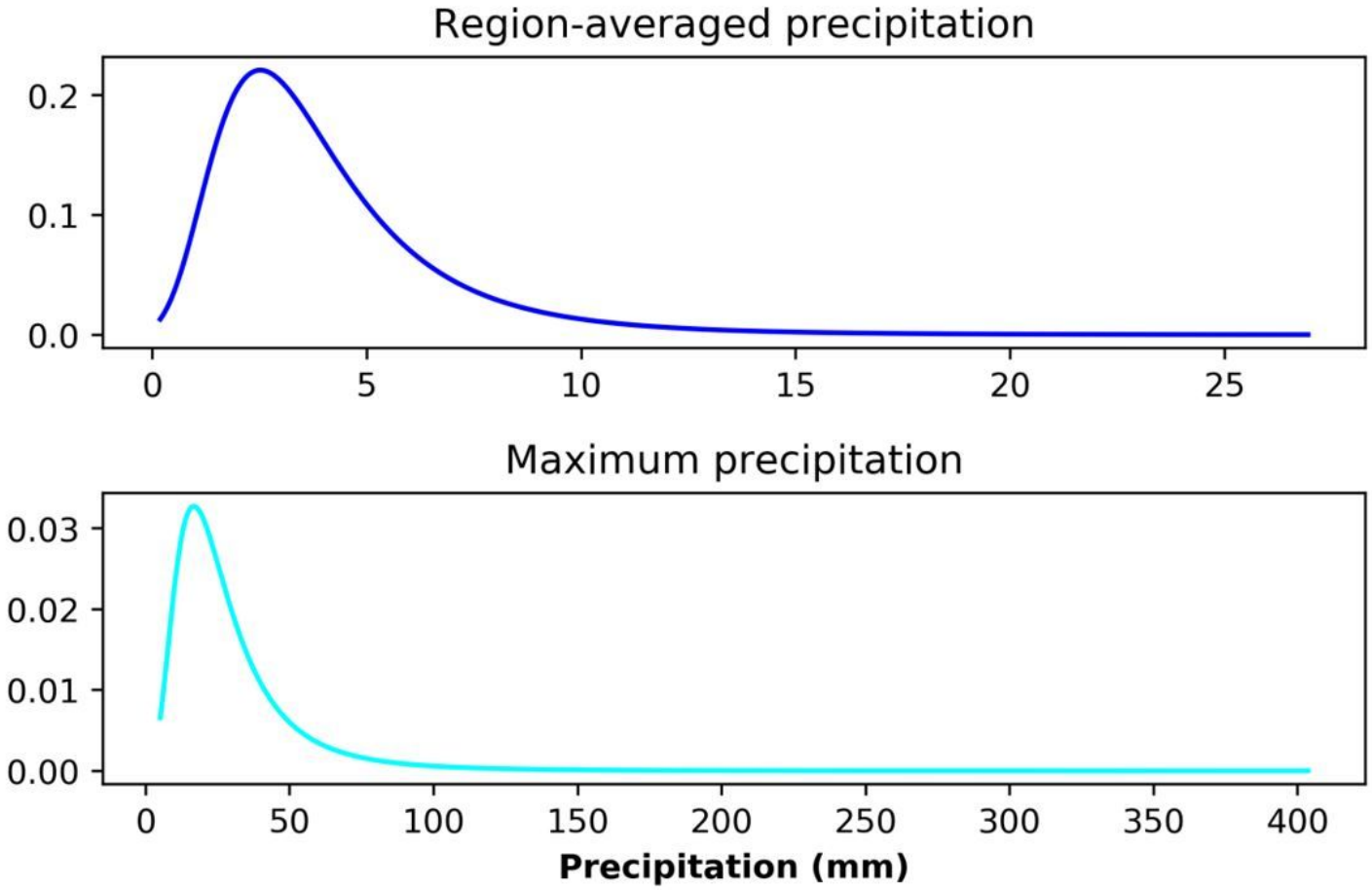

Figure 2

GEV distribution of Region-averaged (figure above) and maximum (figure below) monthly total precipitation for winters from 1988 to 2018. The horizontal axes are precipitation amount in mm, and the vertical axes are probability.

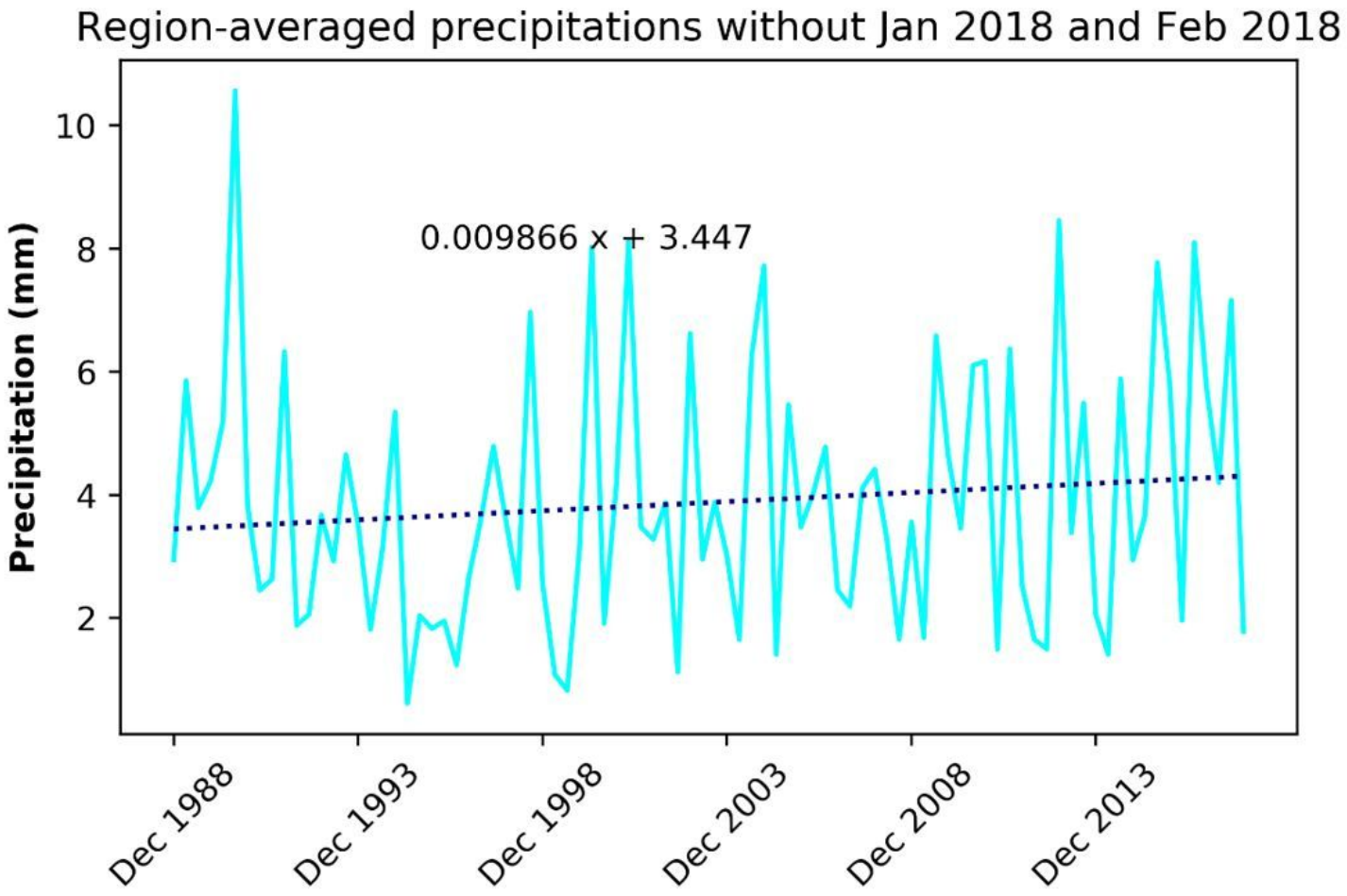

Figure 3

Region-averaged monthly total precipitation without January 2018 and February 2018. The horizontal axis is time line and the vertical axis is precipitation amount in mm. The cyan curve is the Region-averaged monthly total precipitation, and the blue dashed line is the precipitation trend line in first order polynomial fit. The trend line equation is written on the figure.

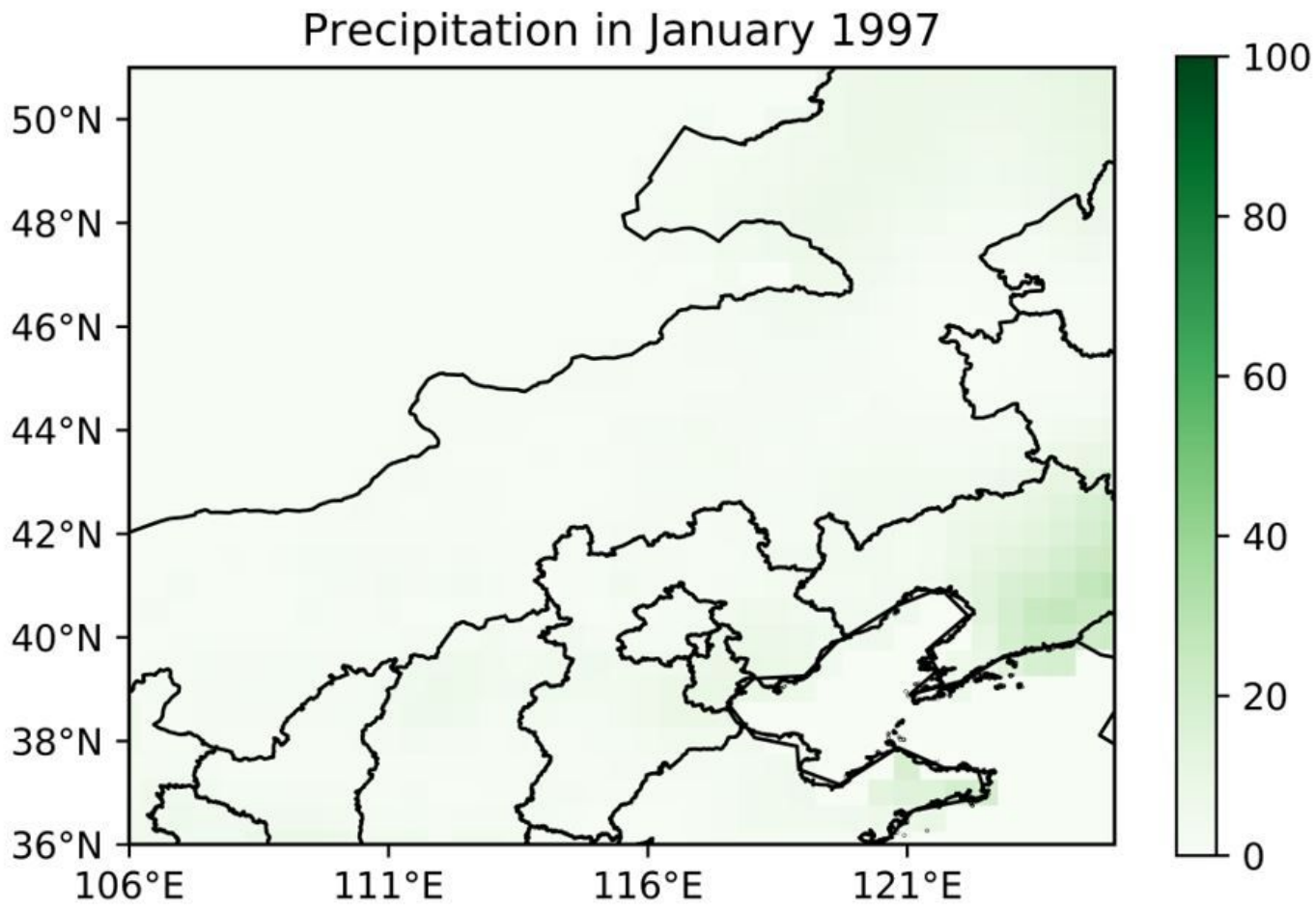

Figure 4

Monthly total precipitation in January 1997 in the Region. The green color illustrate the precipitation amount. The color bar to the right is the precipitation amount with mm as unit.

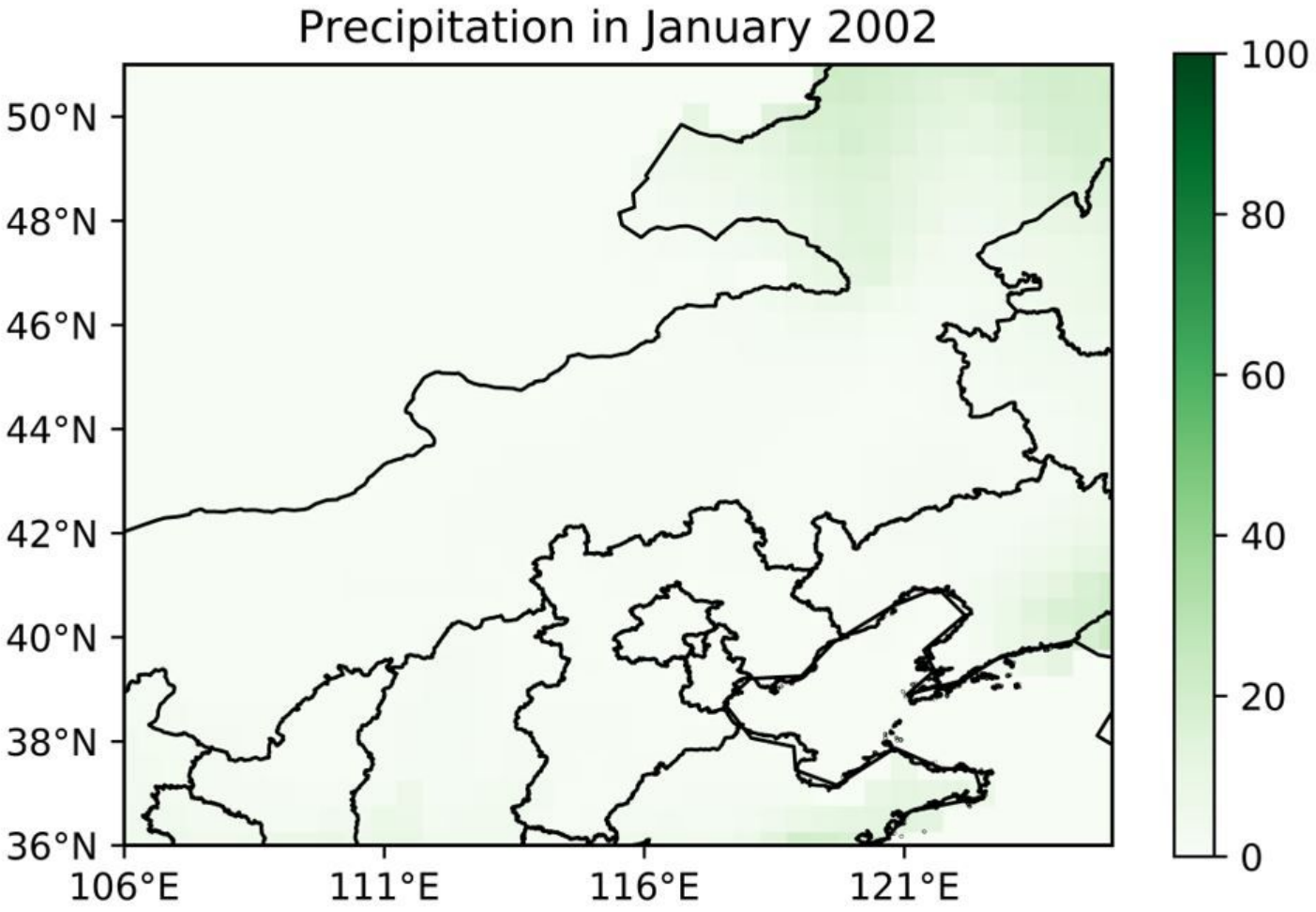

Figure 5

Monthly total precipitation in January 2002 in the Region. The green color illustrate the precipitation amount. The color bar to the right is the precipitation amount with mm as unit.

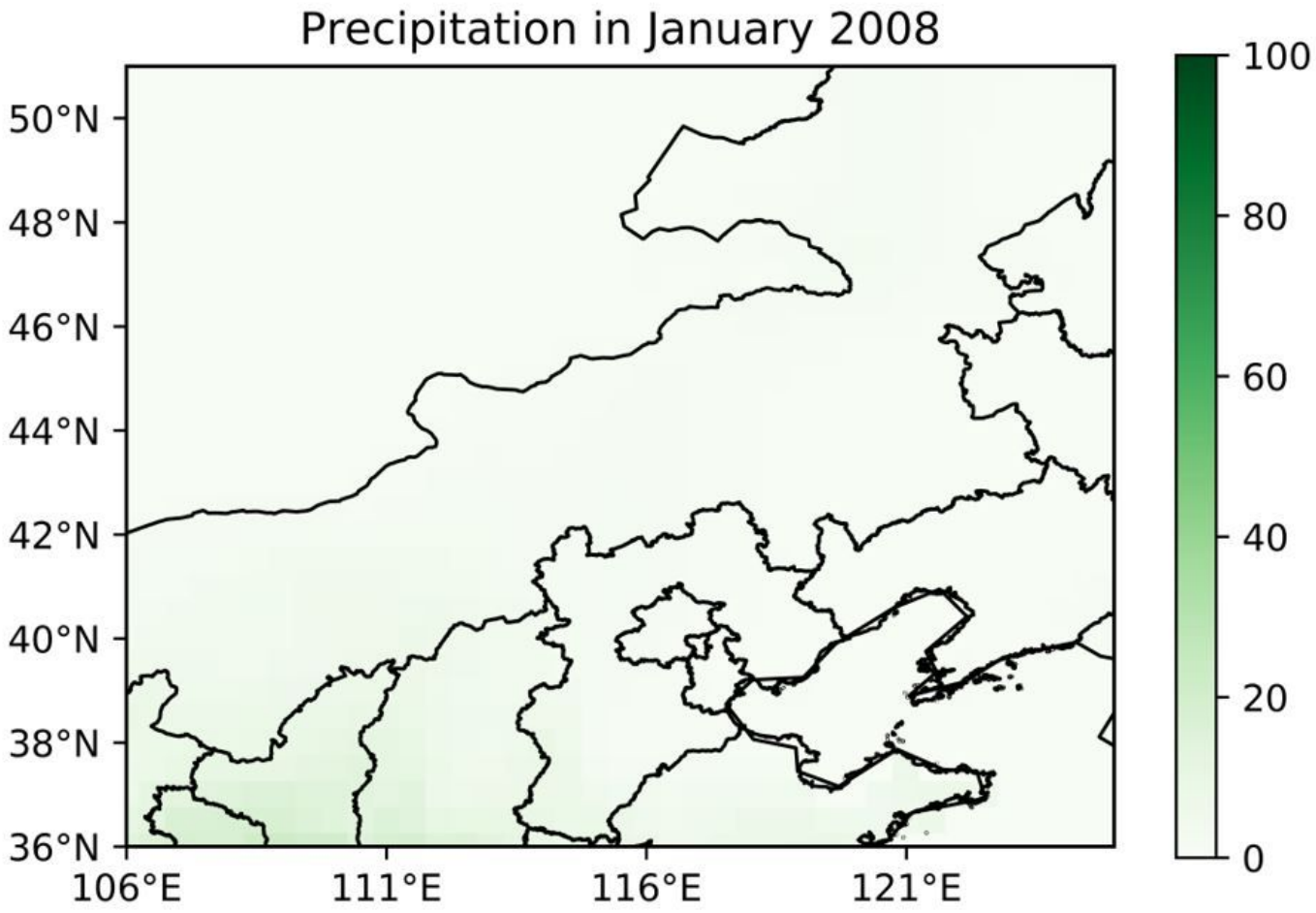

Figure 6

Monthly total precipitation in January 2008 in the Region. The green color illustrate the precipitation amount. The color bar to the right is the precipitation amount with mm as unit.

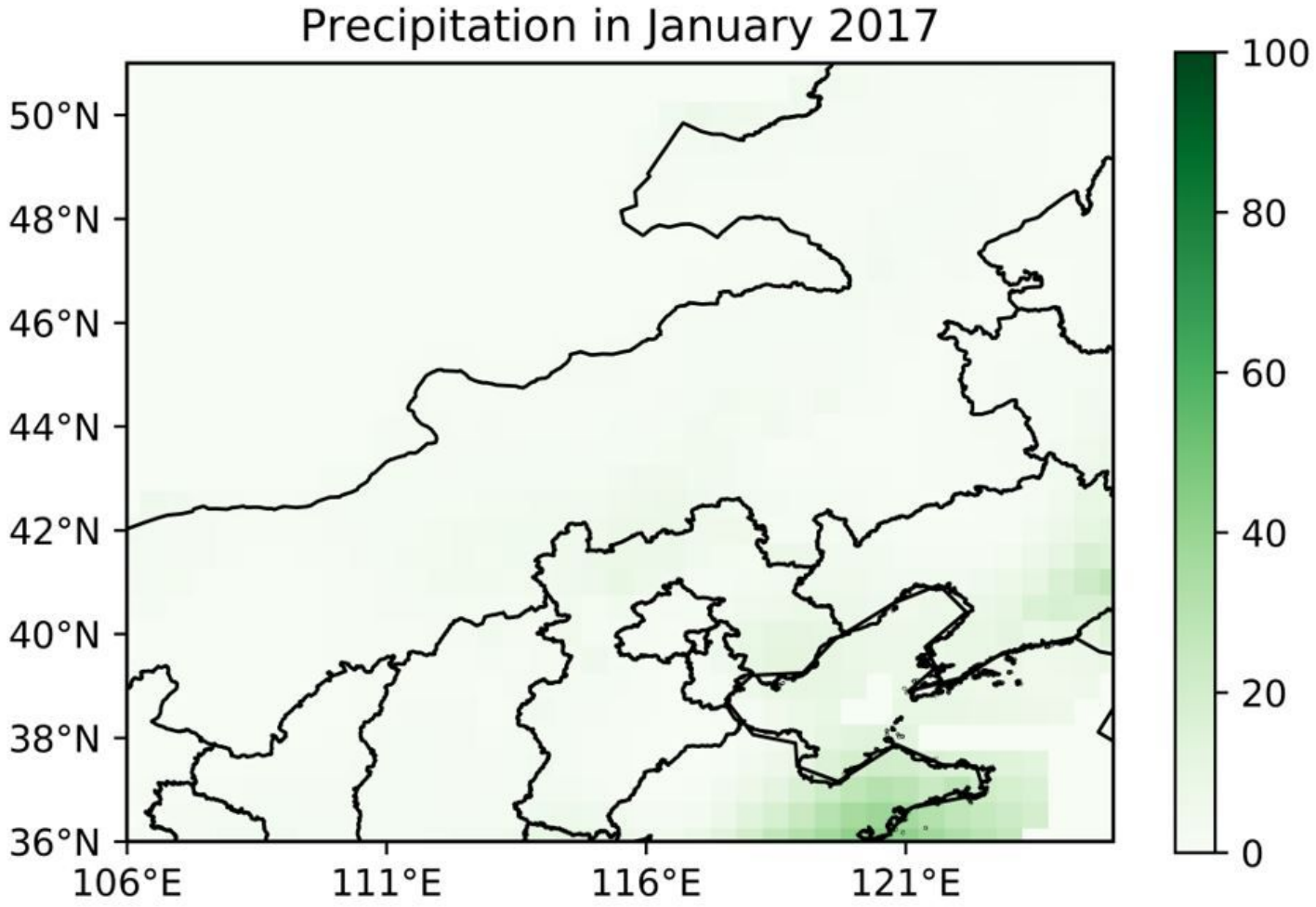

Figure 7

Monthly total precipitation in January 2017 in the Region. The green color illustrate the precipitation amount. The color bar to the right is the precipitation amount with mm as unit.

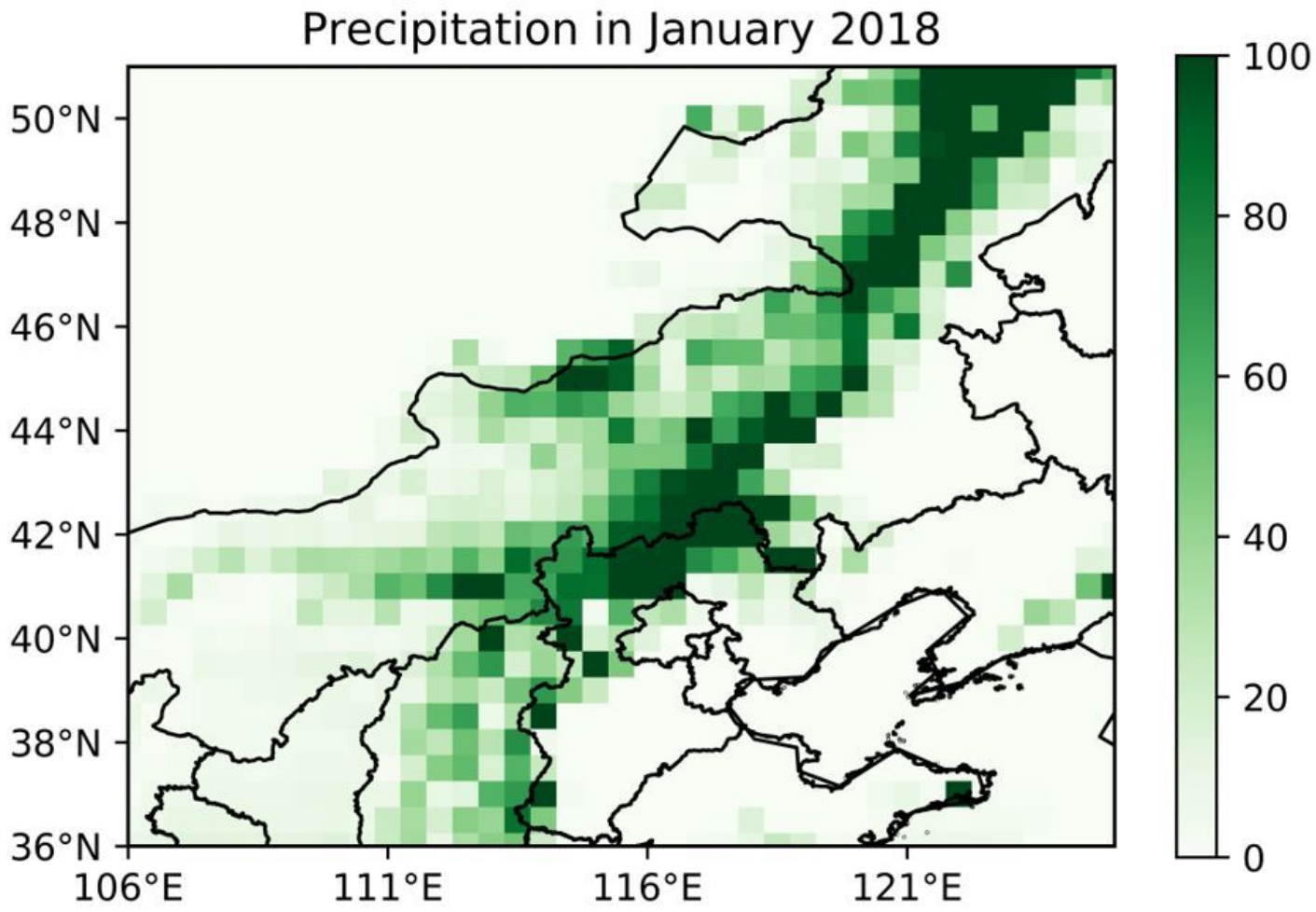

Figure 8

Monthly total precipitation in January 2018 in the Region. The green color illustrate the precipitation amount. The color bar to the right is the precipitation amount with mm as unit.

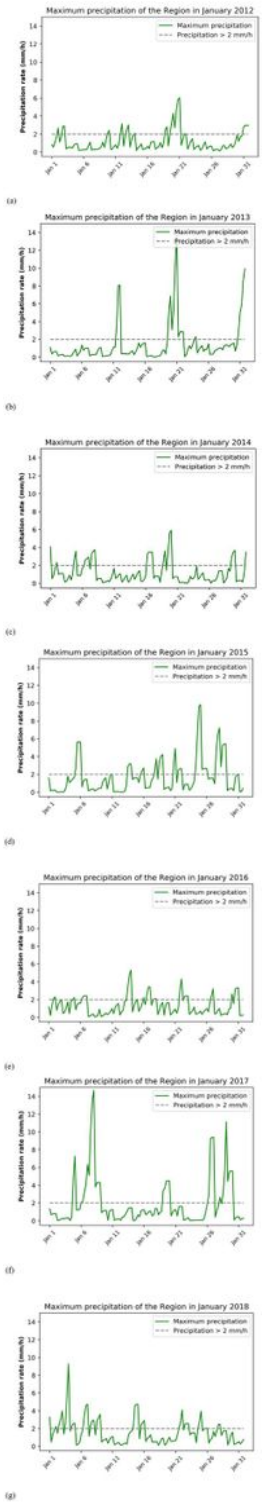

Figure 9

Hourly precipitation rate of the Region for Januaries from 2012 to 2018 (a) – (g). The horizontal axis is the time line from the first day to the last day, and the vertical axis is the precipitation rate with mm/h as unit. The fold line in dark green is the maximum precipitation rate within the Region, and the dashed gray line is the threshold of precipitation rate that equals to 2 mm/h.

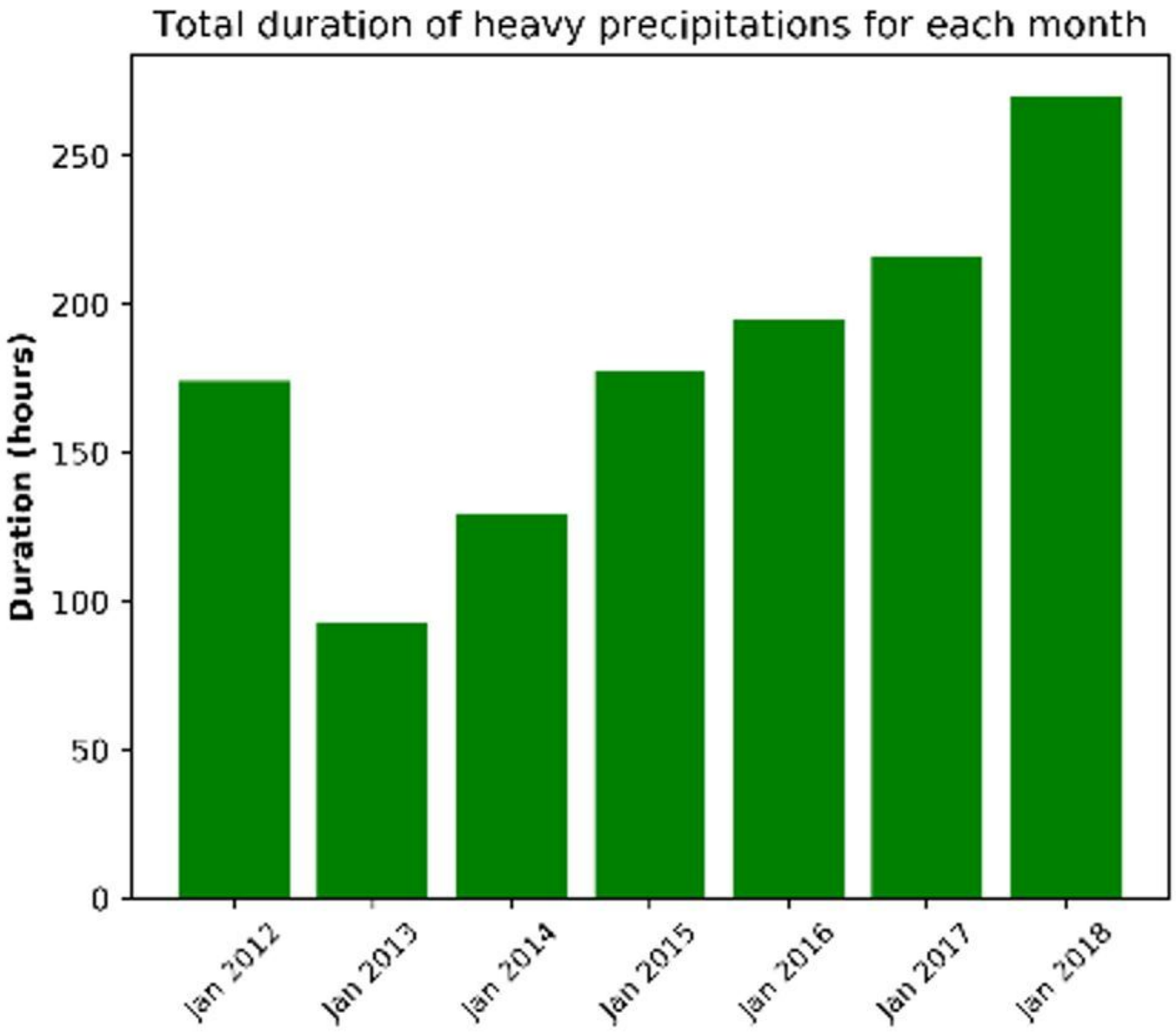

Figure 10

The sum of heavy precipitation durations in January from 2012 to 2018. The horizontal axis is time line, and the vertical axis is the total duration with hours as unit. The dark green bars depict the duration.

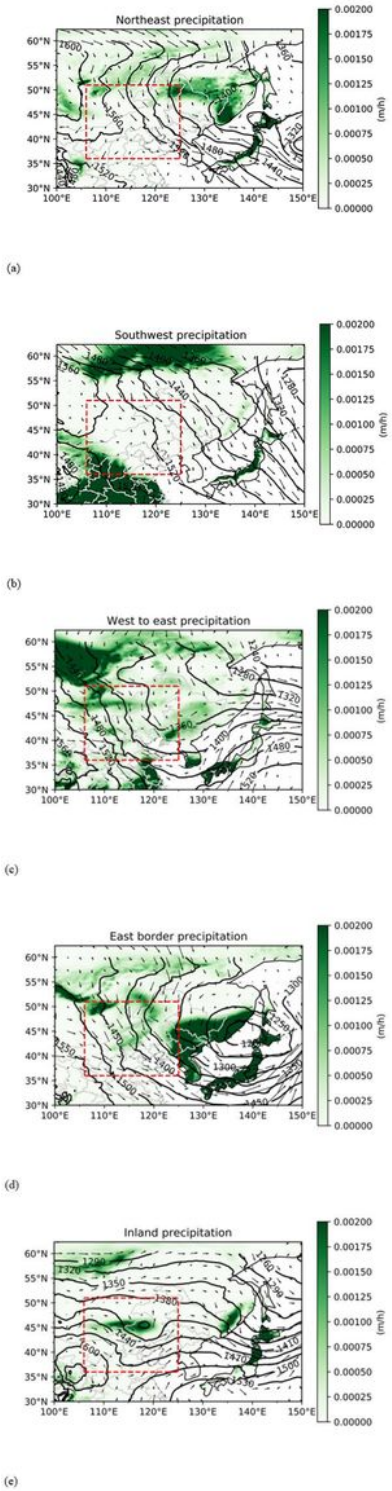

Figure 11

Precipitations with wind field (arrows), geopotential heights (curved lines with numbers on them) and precipitations (dark green patches). The color bar to the right of the figure shows the precipitation rate with m/s as unit. The area is extended for 100 °E – 150 °E, 30 °N – 62°N. The red dashed rectangle limits the Region. There are five types of precipitations named after their locations, and they are Northeast

precipitation (a), Southwest precipitation (b), West to east precipitation (c), East border precipitation (d) and Inland precipitation(e).

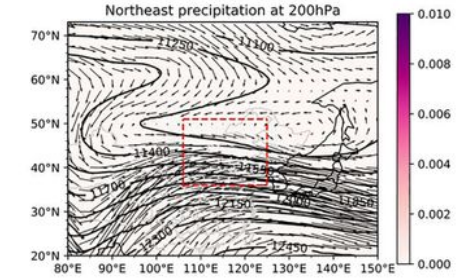

(a)

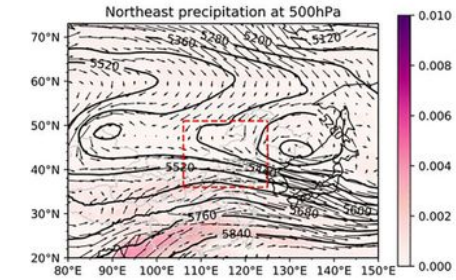

(b)

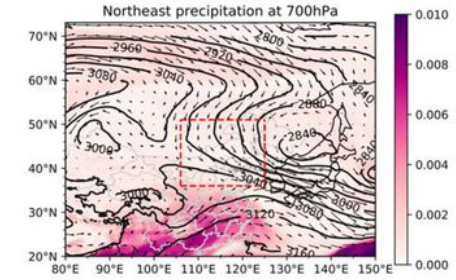

(c)

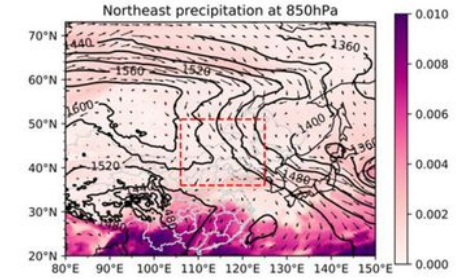

(d)

Figure 12

The Northeast precipitation with wind field (arrows), relative humidity (purple patches) and geopotential height at 200 hPa (a), 500 hPa (b), 700 hPa (c) and 850 hPa (d). The observation area spans 80 °E – 150

°E, 20 °N – 73 °N. The color bar to the right illustrates relative humidity. The red dashed rectangle limits the area of the Region.

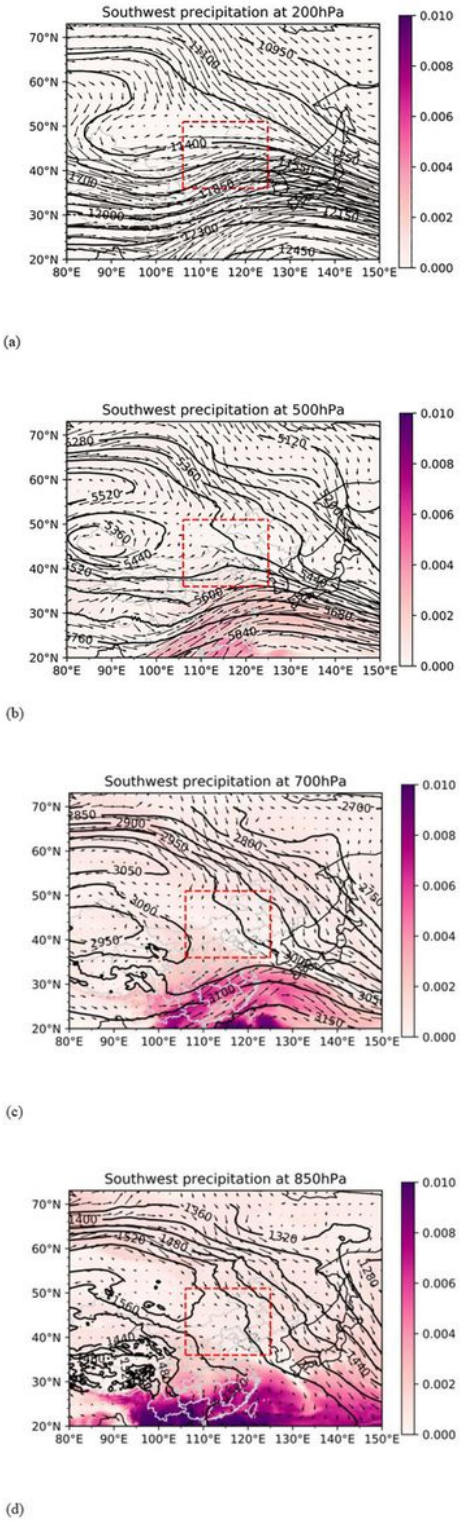

Figure 13

The Southwest precipitation with wind field (arrows), relative humidity (purple patches) and geopotential height at 200 hPa (a), 500 hPa (b), 700 hPa (c) and 850 hPa (d). The observation area spans 80 °E – 150

°E, 20 °N – 73 °N. The color bar to the right illustrates relative humidity. The red dashed rectangle limits the area of the Region.

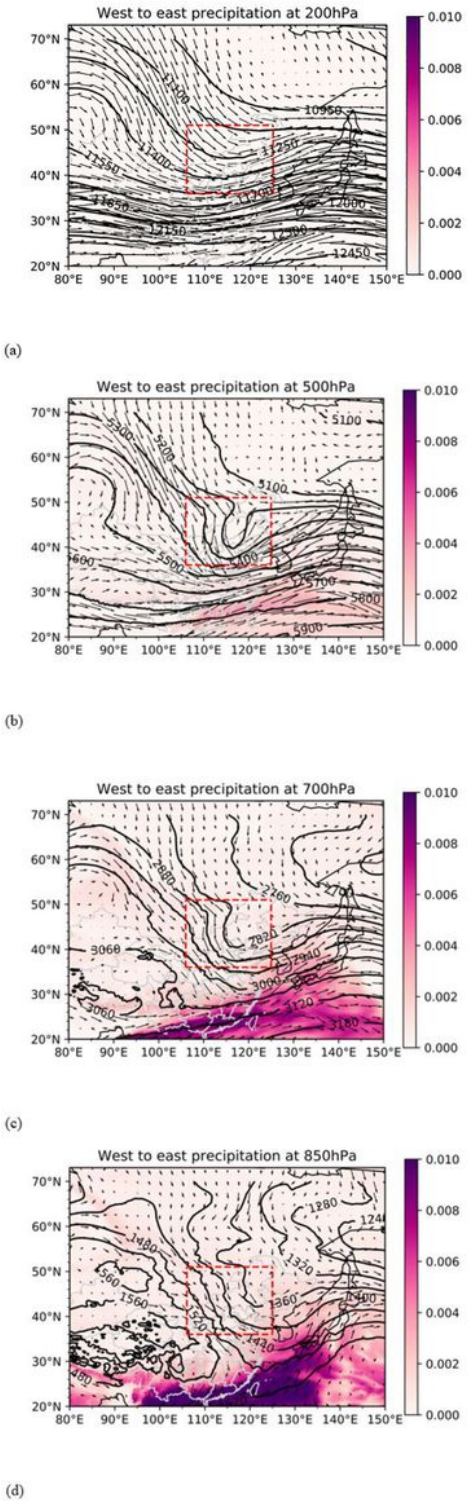

Figure 14

The West to east precipitation with wind field (arrows), relative humidity (purple patches) and geopotential height at 200 hPa (a), 500 hPa (b), 700 hPa (c) and 850 hPa (d). The observation area spans

80 °E – 150 °E, 20 °N – 73 °N. The color bar to the right illustrates relative humidity. The red dashed rectangle limits the area of the Region.

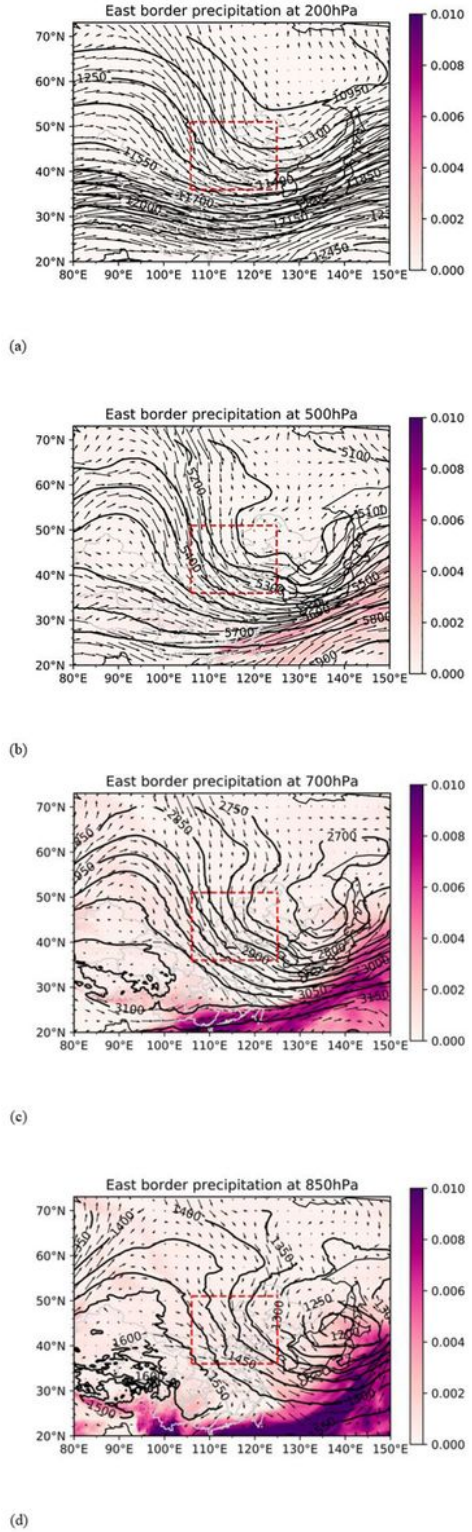

Figure 15

The East border precipitation with wind field (arrows), relative humidity (purple patches) and geopotential height at 200 hPa (a), 500 hPa (b), 700 hPa (c) and 850 hPa (d). The observation area spans 80 °E – 150

°E, 20 °N – 73 °N. The color bar to the right illustrates relative humidity. The red dashed rectangle limits the area of the Region.

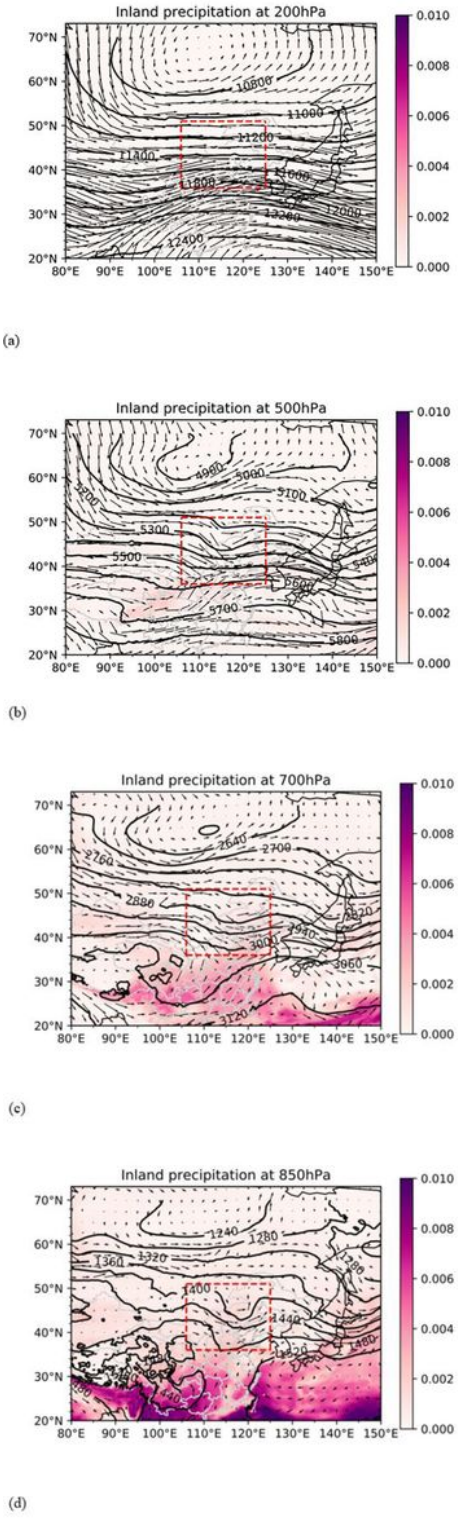

Figure 16

The Inland precipitation with wind field (arrows), relative humidity (purple patches) and geopotential height at 200 hPa (a), 500 hPa (b), 700 hPa (c) and 850 hPa (d). The observation area spans 80 °E – 150

°E, 20 °N – 73 °N. The color bar to the right illustrates relative humidity. The red dashed rectangle limits the area of the Region.